

Passband-Switchable and Frequency-Tunable Dual-Passband Microwave Photonic Filter

Zhejing Jiao  and Jianping Yao 

Abstract—A passband-switchable and frequency-tunable dual passband microwave photonic filter (MPF) implemented using a broadband optical source (BOS) in a delay-line configuration is proposed and experimentally demonstrated. In the proposed MPF, the BOS is sliced by a Mach-Zehnder interferometer (MZI), in which a phase modulator (PM) is incorporated in the upper arm. The phase-modulated light signal combined with an unmodulated light at the output of the MZI is sent through a dispersive delay line and detected at a photodetector (PD). The entire operation is equivalent to a microwave bandpass filter with its central frequency determined by the time delay difference between the two arms of the MZI. To implement a dual passband MPF, a second lower arm with a different arm length corresponding to a different time delay is added. The independent switchability of the passband is realized by controlling the polarization state of the light wave in each of the lower arms to be parallel or orthogonal with that of the upper arm. The independent frequency tunability is achieved by tuning the time delay of each of the lower arms. The proposed MPF is experimentally evaluated. A dual-passband MPF with independent passband switchability and independent frequency tunability is demonstrated. The results show that each of the two passbands can be switched on and off with an extinction ratio of about 20 dB. The passband frequency can also be continuously tuned with a tunable range from 1 to 18 GHz.

Index Terms—Delay line, dual passband microwave photonic filter, frequency tunability, microwave photonics, passband switchability.

I. INTRODUCTION

MICROWAVE photonic filters (MPFs) have been extensively studied in the past few years [1], [2]. Generally, an MPF can be implemented in the incoherent regime using

Manuscript received February 23, 2020; revised April 25, 2020; accepted April 26, 2020. Date of publication April 29, 2020; date of current version October 1, 2020. This work is supported by the Natural Sciences and Engineering Research Council of Canada (NSERC). The work of Z. Jiao was supported in part by the National Natural Science Foundation of China under Grant 61704103, in part by the Shanghai Municipal Commission of Science and Technology, China Project no. 16ZR1412900, and in part by the Key Laboratory of Infrared Imaging Materials and Detectors, Shanghai Institute of Technical Physics, Chinese Academy of Sciences, China Project no. IIMDKFJJ-16-06. (Corresponding author: Jianping Yao.)

Zhejing Jiao is with The Microwave Photonics Research Laboratory, School of Electrical Engineering and Computer Science, University of Ottawa, Ottawa, ON K1N 6N5, Canada, and also with the College of Electronics and Information Engineering, Shanghai University of Electric Power, Shanghai 200090, China (e-mail: jiaojinjin1111@hotmail.com).

Jianping Yao is with The Microwave Photonics Research Laboratory, School of Electrical Engineering and Computer Science, University of Ottawa, Ottawa, ON K1N 6N5 (e-mail: jpyao@uottawa.ca).

Color versions of one or more of the figures in this article are available online at <https://ieeexplore.ieee.org>.

Digital Object Identifier 10.1109/JLT.2020.2991364

a delay-line configuration or in the coherent regime using an optical filter. In the incoherent regime, an MPF usually has a periodic RF spectral response with the period equal to the free spectral range (FSR) [3]–[5]. To avoid having a periodic spectral response, one may use a broadband optical source (BOS) that is spectrally shaped by a Mach-Zehnder interferometer (MZI) having a sinusoidal spectral response [6], [7]. On the other hand, a single passband MPF can be implemented in the coherent regime, in which the single passband is obtained by translating the spectral response of an optical filter to the microwave domain via phase modulation and phase modulation to intensity modulation (PM-IM) conversion. The optical filter can be a phase-shifted fiber Bragg grating (PS-FBG) [8], a micro-ring resonator (MRR) [9], a micro-disk resonator (MDR) [10], or an optical filter based on stimulated Brillouin scattering (SBS) [11].

To implement an MPF with dual passbands in a delay line configuration, two MZIs [12] or an MZI combined with a piece of high birefringence fiber [13] is required. By using multiple MZIs or birefringence fibers, an MPF with multiple passbands can be realized [14], [15]. A dual or multi passband MPF can also be implemented in the coherent regime by using two or multiple optical filters [16]–[18]. For a multi-passband MPF, it is also desired that the passbands can be switchable. For example, in satellite communications systems we may need to enable two passbands or only one passband depending on the application scenario. Although a passband-switchable dual-passband MPF was reported [19], the central frequency of the second passband is always twice the frequency of the first passband, and the passbands cannot be independently switched, which strongly limits the practical applications. The same limitations exist in passband-switchable multi-passband MPFs [14], [15], [20].

In this paper, we propose and experimentally demonstrate for the first time a passband-switchable and frequency-tunable dual-passband MPF with independent frequency switchability and independent frequency tunability using a BOS in a delay line configuration. The spectrum of the BOS is shaped by an MZI with a sinusoidal spectral response. A phase modulator (PM) is incorporated in the upper arm of the MZI to generate a phase-modulated optical signal. The phase-modulated optical signal combined with an unmodulated light wave from the lower arm at the output of the MZI is then sent through a length of dispersive fiber and detected at a photodetector (PD). The entire operation is equivalent to a single passband MPF with its passband frequency determined by the time delay difference between the two arms of the MZI. By incorporating a second lower arm with a different arm length to the MZI,

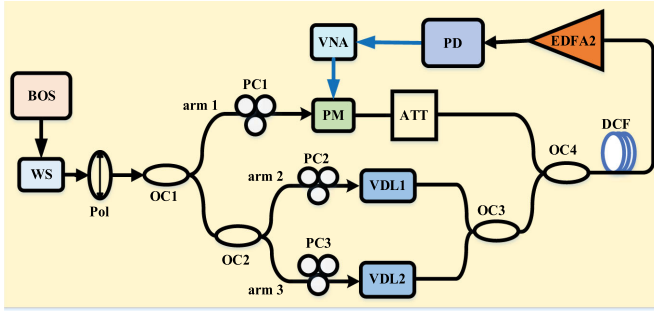


Fig. 1. The schematic of the proposed independent passband-switchable and independent frequency-tunable dual passband MPF. BOS: broadband optical source; WS: waveshaper; Pol: polarizer; OC: optical coupler; PC: polarization controller; PM: phase modulator; VDL: variable optical delay line; Att: attenuator; DCF: dispersion compensating fiber; EDFA: erbium doped fiber amplifier; PD: photodetector; VNA: vector network analyzer.

a dual passband MPF is realized. The independent passband switchability is achieved by controlling the polarization states of the light waves from the upper and the lower arms to make them parallel (corresponding to a passband that is switched on) and orthogonal (corresponding to a passband that is switched off), and the independent frequency tunability of a passband is achieved by tuning the time delay difference between the upper and lower arms. An experiment is performed. The results show that each passband can be independently switched on and off with an extinction ratio of about 20 dB. The central frequency of a passband can also be continuously tuned with a wide tunable range from 1 to 18 GHz.

II. PRINCIPLE

The schematic of the proposed passband-switchable and frequency-tunable dual passband MPF is shown in Fig. 1. An erbium-doped fiber amplifier (EDFA) is used as a BOS. The light wave from the BOS is filtered and flattened by a waveshaper and then linearly polarized by a polarizer, and split into three light waves through two 50:50 optical couplers (OC1 and OC2), with the light wave in the upper arm modulated at a PM, and light waves in the lower arms delayed by two VDLs (VDL1 and VDL2), combined at two other 50:50 OCs (OC3 and OC4), and sent through a dispersion compensating fiber (DCF) and a second EDFA (EDFA2) to a PD. In each arm, a polarization controller (PC) is employed to control the polarization direction of the light wave to make the light wave in the lower arms to be aligned with or orthogonal to that of the upper arm, to achieve independent bandpass switchability. A tunable attenuator (ATT) is used in the upper arm to control the optical power. The frequency response of the MPF is measured by a vector network analyzer (VNA).

Assume the optical field at the input of PC1 is $E(t)$, a phase-modulated signal is generated at the PM which is given by

$$e_1(t) = \vec{e}_1 E(t) e^{jm_p f(t)} \quad (1)$$

where \vec{e}_1 is the polarization direction of the light wave at the input of the PM controlled by PC1, m_p is the phase modulation index and $f(t)$ is the modulation signal, given by $f(t) =$

$V_m \cos(\Omega t)$, where V_m is the amplitude and Ω is the angular frequency of the modulation signal.

The optical fields at the lower two arms after passing through the VDLs (VDL1 and VDL2) can be expressed as

$$e_2(t) = \vec{e}_2 E(t) e^{j\omega t_1} \quad (2.1)$$

$$e_3(t) = \vec{e}_3 E(t) e^{j\omega t_2} \quad (2.2)$$

where \vec{e}_2 and \vec{e}_3 are, respectively, the polarization directions of the light waves at the output of VDL1 and VDL2, which can be controlled by PC2 and PC3, t_1 and t_2 are the time delays introduced by VDL1 and VDL2, respectively, and ω is the angular frequency of the optical carrier.

The electrical fields at the outputs of the three arms combine at OC4, where the combined light wave experiences frequency-dependent time delay τ at the DCF. The time delay τ is given by $\tau = \tau_0 + L\beta_2(\omega - \omega_0)$, where τ_0 is the time delay at the reference frequency ω_0 , L is the length of the DCF, and β_2 is the group velocity dispersion parameter at ω_0 . After passing through the DCF and amplified by EDFA2, the optical signals are converted to electrical signals at the PD. The generated photocurrent at the output of the PD consists of two currents, given by

$$i_{PD}(\Omega) = i_{12}(\Omega) + i_{13}(\Omega) \quad (3)$$

where $i_{12}(\Omega)$ and $i_{13}(\Omega)$ are the currents due to the beating between the sidebands and the carrier from arm 1 and arm 2, and from arm 1 and arm 3, respectively, which are given by

$$i_{12}(\Omega) = \vec{e}_1 \vec{e}_2 \times \begin{cases} R \times P_{ASE} J_1(m_p V) \text{sinc}[(t_1 - \beta_2 L \Omega) \Delta\omega] \\ -R \times P_{ASE} J_1(m_p V) \text{sinc}[(t_1 + \beta_2 L \Omega) \Delta\omega] \end{cases} \quad (4)$$

$$i_{13}(\Omega) = \vec{e}_1 \vec{e}_3 \times \begin{cases} R \times P_{ASE} J_1(m_p V) \text{sinc}[(t_2 - \beta_2 L \Omega) \Delta\omega] \\ -R \times P_{ASE} J_1(m_p V) \text{sinc}[(t_2 + \beta_2 L \Omega) \Delta\omega] \end{cases} \quad (5)$$

where R is the responsivity of the PD, $P_{ASE} = 2E_0^2 \Delta\omega$ is the optical power of the light wave from the BOS, $J_1(\cdot)$ denotes the 1-st order Bessel function of the first kind, and $\Delta\omega$ is the optical bandwidth of the BOS after the waveshaper.

Note that beating between the carrier from a lower arm and the sidebands from the upper arm results in baseband response in the RF spectrum, which is eliminated due to phase modulation in our experiment. In addition, the beating between the carriers from the lower two arms contributes to a DC in the RF spectrum, which is eliminated due to phase modulation and is ignored in (3).

Considering that the modulation signal applied to the PM is $f(t) = V_m \cos(\Omega t)$, the transfer function of the MPF is given by [21]

$$H(\Omega) = \frac{i_{PD}(\Omega)}{V_m/2} \quad (6)$$

As can be seen the frequency response is determined by the two currents in (4) and (5). In (4), there is a Sinc function in its expression, thus the MPF has a passband at a central frequency of

$$\Omega_1 = \frac{t_1}{\beta_2 L} \quad (7)$$

which is caused by the beating between the sidebands from arm 1 and the carrier from arm 2. Similarly, the beating between the sidebands from arm 1 and the carrier from arm 3 results in a second passband at a central frequency of

$$\Omega_2 = \frac{t_2}{\beta_2 L} \quad (8)$$

Thus, the MPF has two passbands. The central frequencies of the two passbands are proportional to the time delays of the lower two arms. By controlling the time delays through tuning VDL1 and VDL2, the frequencies of the two passbands can be independently tuned.

In addition to the independent frequency tunability, the MPF can be independently switched. The independent switchability of the passband is realized by controlling the polarization state of the light wave in each of the two lower arms to be parallel or orthogonal to that of the upper arm. The products between two vectors, $\vec{e}_1 \vec{e}_2$ and $\vec{e}_1 \vec{e}_3$ in (4) and (5) represent the beating strengths between the two signals from the upper arm and one of the two lower arms, which are determined by their polarization directions and can be controlled by the three PCs. A maximum beating strength is obtained if the signals from the arms are with the same polarization directions and no beating signal is obtained if they are orthogonally polarized. Mathematically, the products of two vectors can be written as

$$\vec{e}_1 \vec{e}_2 = \cos \theta_1 \quad (9.1)$$

$$\vec{e}_1 \vec{e}_3 = \cos \theta_2 \quad (9.2)$$

where θ_1 is the polarization angle difference between the two signals from arm 1 and arm 2 and θ_2 is the polarization angle difference between the two signals from arm 1 and arm 3. When PC1 in arm 1 is tuned to make the polarization direction of the light in that arm be parallel to the principal axis of the PM, the value of $\cos \theta_1$ can be changed by tuning PC2 in arm 2 between 1 and 0, corresponding to a maximum and zero beating signal. The corresponding passband of the MPF is then switched between the ON and OFF states, as illustrated in Fig. 2. By tuning PC3 in arm 3 the same way, the 2nd passband of the MPF can be switched between the ON and OFF states.

As can be seen, the tunability and switchability of the two passbands of the MPF can be realized by tuning the VDLs and the PCs in the three arms.

Note that an incoherent BOS is used in the MPF. For an MPF with a delay-line configuration, to avoid optical interference, the light source must be incoherent [1, 2]. Note also that the light waves in the three arms need to be linearly polarized, and the polarization direction of the light wave in the upper arm should be parallel or orthogonal to that of the light wave in one of the lower arm, to maximize or minimize the beating, leading to the passband ON/OFF switchability.

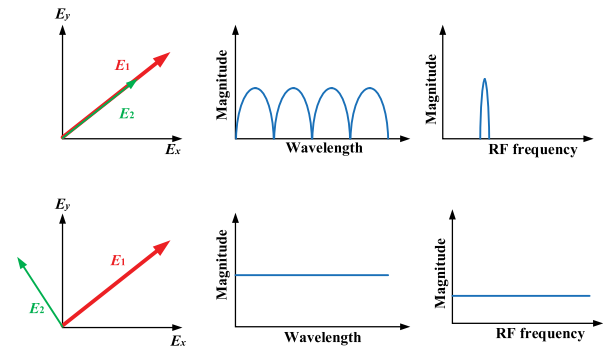


Fig. 2. Illustration of the optical and RF spectra for parallel (up) and orthogonal (bottom) polarization directions between arm 1 and arm 2.

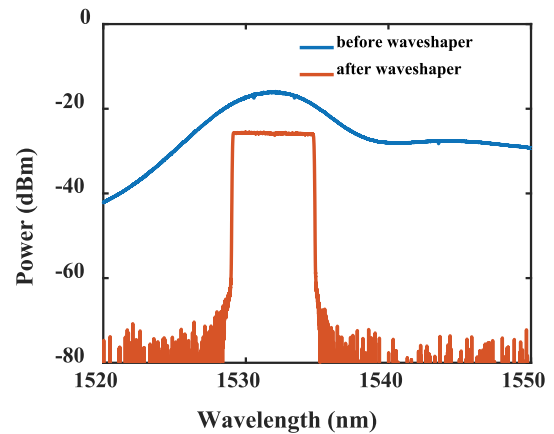


Fig. 3. The spectrum of the light from the BOS (blue) and the spectrum after spectral shaping by the waveshaper (red).

III. EXPERIMENTAL RESULTS AND ANALYSIS

An experiment based on the configuration in Fig. 1 is performed. The spectrum of the BOS, which is generated by an EDFA (EDFA1), is shown in Fig. 3 as blue line. The spectrum is then shaped by the waveshaper (Finisar 4000S). The shaped spectrum has a flat response, shown in Fig. 3 as red line, which has a spectrum width of about 5.7 nm centered at 1531.73 nm. The PM (Thorlabs) has a bandwidth of 40 GHz and PC1 is placed before the PM to minimize the polarization dependent loss. PC2 and PC3 are used to tune the polarization directions of the light waves in arm 2 and arm 3. Due to only one VDL is available at the time of experiment, a single VDL (General Photonics) is employed which is incorporated in arm 3 (VDL2). VDL2 has a tuning range from 0 to 600 ps, corresponding to a length change of 18 cm in vacuum. The DCF has a total dispersion of -1020 ps/nm with a fiber length of 6.25 km ($\beta_2 L = 12.67 \times 10^{-22}$ ps²). The PD (New Focus) used in the experiment has a bandwidth of 20 GHz.

The experiment is performed in three steps. In step A, the independent switchability of the two passbands at fixed centre frequencies is demonstrated. In step B, both passbands are switched on and the centre frequency of one passband is tuned to demonstrate the independent frequency tunability. In step C, the passbands are switched between ON and OFF and the central

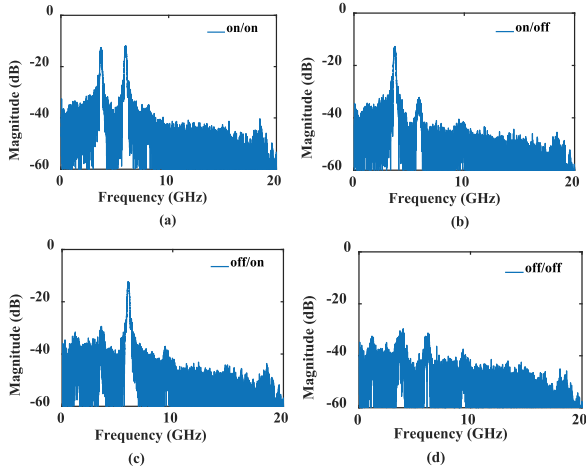


Fig. 4. The switchability of the two passbands at f_1 and f_2 . (a) Both passbands are switched on. (b) The 1st passband at f_1 is switched on and the 2nd passband at f_2 is switched off. (c) The 1st passband at f_1 is switched off and the 2nd passband at f_2 is switched on. (d) Both passbands are switched off.

frequency of one passband is tuned to demonstrate both the independent passband switchability and independent frequency tunability.

A. Passband Switchability

To demonstrate the independent passband switchability, the lengths of arm 2 and arm 3 are fixed and PC2 and PC3 are tuned. The length difference between arm 1 and arm 2 is fixed at about 6 mm, corresponding to a passband (we call it the first passband) frequency of the MPF at 3.7 GHz, which is calculated based on

$$f_1 = \frac{t_1}{2\pi\beta_2 L} = \frac{n\Delta L_1}{2\pi c} \times \frac{1}{\beta_2 L} \quad (10)$$

where n is the refractive index of the fiber at 1530 nm which is 1.47 in the calculation; ΔL_1 is the length difference between arm 1 and arm 2 which is fixed at 6 mm, and c is the speed of light in vacuum.

In arm 3, the length of the VDL2 is set to 10.8 cm, corresponding to a central frequency of the passband (we call it the second passband) at $f_2 = 6$ GHz. PC1 in arm 1 is tuned to minimize the polarization dependent loss. Then, PC2 in arm 2 is tuned to control the beating strength between the signals from arm 1 and arm 2 to switch the passband at f_1 to be ON or OFF. PC3 in arm 3 is used to switch the passband at f_2 to be ON or OFF. The two passbands can be switched independently by tuning the two PCs. Fig. 4 shows the four different states of the two passbands. In Fig. 4(a), both passbands are switched on. The 3-dB bandwidths of the passbands are about 169.6 and 174.6 MHz. The bandwidth can be smaller by using a BOS with wider bandwidth. The extinction ratio between the ON/OFF and OFF/ON states of the two passbands in Fig. 4(b) and (c) are about 20 dB. The extinction ratio of the passband is strongly related to the beating strength between the signals from arm 1 and the lower two arms, which is determined by their polarization angle differences. In our experiment, the length of each arm is about 34 m due to fiber pigtailed and single-mode fibers employed to match the length difference among the three arms. It is hard

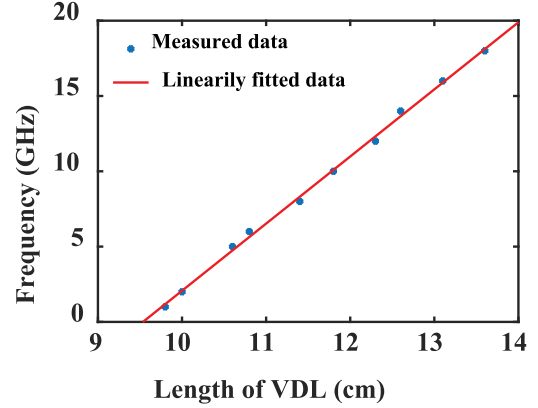


Fig. 5. The tuning of the central frequency of the second passband when the length of arm 3 is tuned via tuning VDL2.

to strictly keep the polarization in these single-mode fibers, which decreases the contrast ratios. The extinction ratio can be improved if the polarization directions of the light waves in the arms can be kept strictly parallel or orthogonal.

In Fig. 4(d), the two passbands are both switched off, which can be done either by tuning PC1 to make the incident light wave to have a polarization direction orthogonal to the principal axis of the PM, to have a highest polarization-dependent loss, or by tuning PC2 and PC3 to minimize the beating strength. We may notice that in addition to the two off passbands at f_1 and f_2 , two low peaks at around 1.1 and 9.3 GHz are observed, as shown in Fig. 4(d), which are caused due to the weak TE mode supported by PM. Ideally, the PM will only support the TM mode and fully suppress the TE mode.

B. Frequency Tunability

The independent frequency tunability of the MPF is also experimentally studied. By tuning the two VDLs in the lower arms, the central frequency of the two passbands can be independently tuned. In this step, the three PCs are adjusted to have the maximum beating strength. The length of arm 2 is fixed to make the central frequency of the first passband fixed at 3.7 GHz. Then, we tune the length of arm 3 via tuning VDL2 from 9.8 to 10.8 cm, corresponding to a central frequency change of the second passband from 1 to 6 GHz. Then the length of VDL2 is tuned from 10.8 to 13.6 cm with a tuning step of 0.46 cm, corresponding to a change in the central frequency of the passband from 6 to 18 GHz with a frequency interval of 2 GHz. The passband frequency is linearly increased with the increase of the length of VDL2, as shown in Fig. 5. The spectra of the MPF when the central frequency of the second passband is tuned are shown in Fig. 6. To avoid the overlap of the two passbands, the second passbands between 1 and 6 GHz are not plotted in Fig. 6. It is seen that the second passband can be continuously tuned from 1 to 18 GHz. During the tuning, the first passband is fixed at 3.7 GHz without being affected, confirming the independent tunability. The 3-dB bandwidth of the second passband when tuned is slightly increased with the increase of its central frequency due to the dispersion of the DCF [22]. The magnitude of the passband is decreased about 12 dB from 6 to

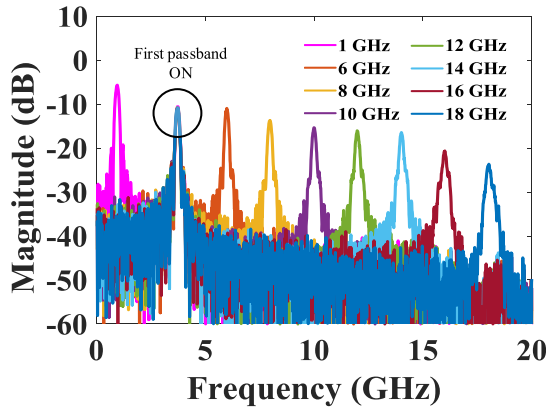


Fig. 6. Both passbands are switched on. The first passband is fixed at 3.7 GHz while the second passband is tuned from 1 to 18 GHz by tuning VDL2.

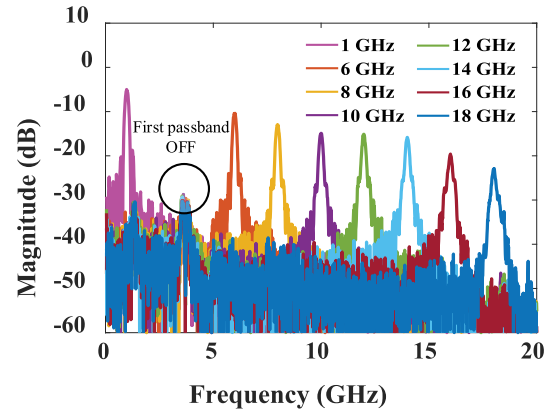


Fig. 8. The first passband is OFF with its central frequency fixed at 3.7 GHz and the second passband is ON and tuned from 1 to 18 GHz by tuning VDL2.

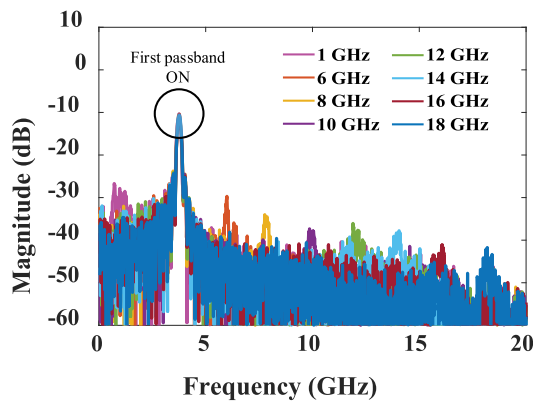


Fig. 7. The first passband is ON with its central frequency fixed at 3.7 GHz, and the second passband is OFF, and tuned from 1 to 18 GHz by tuning VDL2.

18 GHz. This is mainly caused by the nonflat spectral responses of the PD and the two electrical amplifiers (EAs) before the PD.

Note that in the experiment, the frequency tunability of the first passband is not performed due to the lack of a second VDL. In fact, the frequency tunability of the first passband is the same as that of the second passband and can be realized if a second VDL is available and incorporated in arm 2.

C. Switchability and Tunability

Then, the passbands are switched on and off and the central frequency of one passband is tuned to demonstrate both the independent passband switchability and independent frequency tunability.

Firstly, the first passband at 3.7 GHz is switched on and fixed, and the second passband is switched off by tuning PC3. The length of VDL2 in arm 3 is tuned from 9.8 to 13.6 cm by again a tuning step of 0.46 cm. The results are shown in Fig. 7. The magnitude of the second passband is highly suppressed, which are from -29.71 dB at 6 GHz to -42.18 dB at 18 GHz while the magnitude of the passband at 3.7 GHz is kept unchanged. The extinction ratio is maintained more than 20 dB during tuning. We should emphasize that during the tuning the central frequency of the first passband is always kept at 3.7 GHz, further demonstrating the independent switchability and

tunability. Then, the first passband at 3.7 GHz is switched off by tuning PC2 and the second passband is switched on by tuning PC3. Again, VDL2 is tuned from 9.8 to 13.6 cm. The results are shown in Fig. 8. The central frequency of the second passband is tuned from 1 to 18 GHz while the first passband at 3.7 GHz is kept off, indicating again the independent switchability and tunability.

IV. DISCUSSION AND CONCLUSION

The key novelty of the approach is the ability of the MPF to perform independent passband switching and independent frequency tuning, which are two important features for applications, such as in satellite communications and radar systems where one or two passbands need to be enabled or disabled.

In the demonstration, the MPF was implemented with two passbands. To implement an MPF with more than two passbands, more lower arms need to be included. Again, a PC is needed in each of the lower arms to control the polarization direction of the light wave in the arm to achieve independent passband switchability and a VDL is needed to tune the time delay to perform independent frequency tunability.

In summary, a passband switchable and frequency tunable dual-passband MPF was proposed and experimentally demonstrated. The key contribution of the work is that independent passband switchability and independent frequency tunability of an MPF was demonstrated for the first time. The switchability of passband was realized by controlling the polarization state of the light wave in each of the lower arms to be parallel or orthogonal to that of the upper arm. The independent frequency tunability was achieved by tuning the time delay of each of the lower arms. The proposed MPF was experimentally evaluated. A dual-passband MPF with independent passband switchability and independent frequency tunability was demonstrated. The results show that each of the two passbands could be switched on and off independently with an extinction ratio of about 20 dB. The passband frequency could also be independently and continuously tuned with a tunable range from 1 to 18 GHz. The MPF demonstrated has two passbands, but it is scalable to have multiple passbands, which can find applications where switchable multiple passband microwave filters are required.

REFERENCES

- [1] J. Capmany, B. Ortega, and D. Pastor, "A tutorial on microwave photonic filters," *J. Lightw. Technol.*, vol. 24, no. 1, pp. 201–228, Jan. 2006.
- [2] J. P. Yao, "Microwave photonics," *J. Lightw. Technol.*, vol. 27, no. 3, pp. 314–335, Feb. 2009.
- [3] J. Sancho *et al.*, "Integrable microwave filter based on a photonic crystal delay line," *Nat. Commun.*, vol. 3, Sep. 2012, Art. no. 1075.
- [4] Y. Dai and J. P. Yao, "Nonuniformly-spaced photonic microwave delay-line filter," *Opt. Express*, vol. 16, no. 7, pp. 4713–4718, Mar. 2008.
- [5] J. Jing, X. Wang, and L. Lu, "Reconfigurable RF notch filter based on an integrated silicon optical true time delay line," *J. Phys D: Appl. Phys.*, vol. 52, no. 19, May 2019, Art. no. 194001.
- [6] J. Mora, B. Ortega, A. Diez, J. Cruz, M. V. Andres, J. Capmany, and D. Pastor, "Photonic microwave tunable single-bandpass filter based on a Mach-Zehnder interferometer," *J. Lightw. Technol.*, vol. 24, no. 7, pp. 2500–2509, Jul. 2006.
- [7] X. Xue, X. Zheng, H. Zhang, and B. Zhou, "Widely tunable single-bandpass microwave photonic filter employing a non-sliced broadband optical source," *Opt. Express*, vol. 19, no. 19, pp. 18423–18429, Sep. 2011.
- [8] W. Li and J. P. Yao, "A wideband frequency-tunable optoelectronic oscillator incorporating a tunable microwave-photonic filter based on phase-modulation to intensity-modulation conversion using a phase-shifted fiber Bragg grating," *IEEE Trans. Microw. Theory Tech.*, vol. 60, no. 6, pp. 1735–1742, Jun. 2012.
- [9] X. Xue, Y. Xuan, H. Kim, J. Wang, D. E. Leaird, M. Qi, and A. M. Weiner, "Programmable single-bandpass photonic RF filter based on Kerr Comb from a microring," *J. Lightw. Technol.*, vol. 32, no. 20, pp. 3557–3565, Oct. 2014.
- [10] W. Zhang and J. P. Yao, "An on-chip silicon photonic integrated frequency-tunable bandpass microwave photonic filter," *Opt. Lett.*, vol. 43, no. 15, pp. 3622–3625, Aug. 2018.
- [11] S. Hu, L. Li, X. Yi, and C. Yu, "Ultraflat widely tuned single bandpass filter based on stimulated Brillouin scattering," *IEEE Photon. Technol. Lett.*, vol. 26, no. 14, pp. 1466–1469, Jul. 2014.
- [12] L. Huang *et al.*, "Microwave photonic filter with multiple independently tunable passbands based on a broadband optical source," *Opt. Express*, vol. 23, no. 20, pp. 25539–25551, Sep. 2015.
- [13] J. Ge and M. P. Fork, "Optically controlled fast reconfigurable microwave photonic dual-band filter based on nonlinear polarization rotation," *IEEE Trans. Microw. Theory Tech.*, vol. 65, no. 1, pp. 253–259, Jan. 2017.
- [14] Y. Jiang *et al.*, "A selectable multiband bandpass microwave photonic filter," *IEEE Photon. J.*, vol. 5, no. 3, Jun. 2013, Art. no. 5500509.
- [15] R. Wu *et al.*, "Tunable and selectable multipassband microwave photonic filter utilizing reflective and cascaded fiber Mach-Zehnder interferometers," *J. Lightw. Technol.*, vol. 35, no. 13, pp. 2660–2668, Jul. 2017.
- [16] L. Wang, M. Li, N. Zhu, and W. Li, "Switchable microwave photonic filter between dual-notch and dual-passband responses," *IEEE Photon. Technol. Lett.*, vol. 31, no. 21, pp. 1894–1897, Nov. 2018.
- [17] S. Hu, L. Li, and X. Yi, "Tunable dual-passband microwave photonic filter based on stimulated Brillouin scattering," *IEEE Photon. Technol. Lett.*, vol. 29, no. 3, pp. 330–333, Feb. 2017.
- [18] L. Gao, J. Zhang, X. Chen, and J. P. Yao, "Microwave photonic filter with two independently tunable passbands using a phase modulator and an equivalent phase-shifted fiber Bragg grating," *IEEE Trans. Microw. Theory Tech.*, vol. 62, no. 2, pp. 380–387, Feb. 2014.
- [19] H. Chen *et al.*, "Switchable and tunable microwave frequency multiplication based on a dual-passband microwave photonic filter," *Opt. Express*, vol. 23, no. 8, pp. 9835–9843, Apr. 2015.
- [20] J. Ge and M. P. Fork, "Reconfigurable RF multiband filter with widely tunable passbands based on cascaded optical interferometric filter," *J. Lightw. Technol.*, vol. 36, no. 14, pp. 2933–2939, Jul. 2018.
- [21] J. Zhang, L. Gao, and J. P. Yao, "Tunable optoelectronic oscillator incorporating a single passband microwave photonic filter," *IEEE Photon. Technol. Lett.*, vol. 26, no. 4, pp. 326–329, Feb. 2014.
- [22] X. Xue, X. Zheng, H. Zhang, and B. Zhou, "Analysis and compensation of third-order dispersion induced RF distortions in highly reconfigurable microwave photonic filters," *J. Lightw. Technol.*, vol. 31, no. 13, pp. 2263–2270, Jul. 2013.

Zhejing Jiao received the Ph.D. degree in electrical engineering from Concordia University, Montreal, QC, Canada in Sept. 2014. In 2015, she joined the College of Electronics and Information Engineering, Shanghai University of Electric Power, Shanghai, China as a Lecture. She is currently a Visiting Scholar with the Microwave Photonics Research Laboratory, School of Electrical Engineering and Computer Science, University of Ottawa, ON, Canada. Her current research includes semiconductor mode-locked lasers and microwave photonics for wireless communications.

Jianping Yao (Member, IEEE) received the his Ph.D. degree in electrical engineering from the Université de Toulon et du Var, Toulon, France in 1997. He is a Distinguished University Professor and University Research Chair with the School of Electrical Engineering and Computer Science, University of Ottawa, Canada. From 1998 to 2001, he was at with the School of Electrical and Electronic Engineering, Nanyang Technological University, Singapore, as an Assistant Professor. In 2001, he joined the School of Electrical Engineering and Computer Science, University of Ottawa as an Assistant Professor, where he was promoted to a Associate Professor in 2003, and a Full Professor in 2006. He was appointed as the University Research Chair in Microwave Photonics in 2007. In 2016, he was conferred the title of Distinguished University Professor at the University of Ottawa. From 2007 to 2010 and from 2013 to 2016, he was the Director of the Ottawa-Carleton Institute for Electrical and Computer Engineering.

He has authored and co-authored more than 620 research papers including more than 360 papers in peer-reviewed journals and more than 260 papers in conference proceedings. Prof. Yao is the Editor-in-Chief of IEEE Photonics Technology Letters, a Topical Editor of Optics Letters, an Associate Editor of Science Bulletin, a Steering Committee Member of the IEEE Journal of Lightwave Technology, and an Advisory Editorial Board Member of Optics Communications. He was a Guest Editor of a Focus Issue on Microwave Photonics in Optics Express in 2013, a Lead-Editor of a Feature Issue on Microwave Photonics in Photonics Research in 2014, and a Guest Editor of a Special Issue on Microwave Photonics in the IEEE Journal of Lightwave Technology in 2018. He is currently the Chair of the IEEE Photonics Ottawa Chapter and is the Technical Committee Chair of IEEE MTT-3 Microwave Photonics. He was a member of the European Research Council Consolidator Grant Panel in 2016, the Qualitative Evaluation Panel in 2017, and a member of the National Science Foundation Career Awards Panel in 2016. He was also a chair of a number of international conferences, symposia, and workshops, including the Vice Technical Program Committee (TPC) Chair of the 2007 IEEE Topical Meeting on Microwave Photonics, TPC Co-Chair of the 2009

and 2010 Asia-Pacific Microwave Photonics Conference, TPC Chair of the High-Speed and Broadband Wireless Technologies Subcommittee of the IEEE Radio Wireless Symposium 2009-2012, TPC Chair of the Microwave Photonics Subcommittee of the IEEE Photonics Society Annual Meeting 2009, TPC Chair of the 2010 IEEE Topical Meeting on Microwave Photonics, General Co-Chair of the 2011 IEEE Topical Meeting on Microwave Photonics, TPC Co-Chair of the 2014 IEEE Topical Meetings on Microwave Photonics, and General Co-Chair of the 2015 and 2017 IEEE Topical Meeting on Microwave Photonics. He was also a committee member for a number of international conferences, such as IPC, OFC, BGPP, and MWP. He is the recipient of the 2005 International Creative Research Award of the University of Ottawa, the 2007 George S. Glinski Award for Excellence in Research, a Natural Sciences and Engineering Research Council of Canada Discovery Accelerator Supplements Award in 2008, an inaugural OSA Outstanding Reviewer Award in 2012, and the Award for Excellence in Research 2017-2018 at the University of Ottawa. He was one of the top ten reviewers of IEEE/OSA Journal of Lightwave Technology (2015–2016). He was an IEEE MTT-S Distinguished Microwave Lecturer for 2013–2015. He is a registered Professional Engineer of Ontario. He is a Fellow of the Optical Society of America, the Canadian Academy of Engineering, and the Royal Society of Canada.